nature neuroscience

Astrocyte-mediated control of cerebral blood flow

Takahiro Takano[1], Guo-Feng Tian[1], Weiguo Peng[1], Nanhong Lou[1], Witold Libionka[1,2], Xiaoning Han[1] & Maiken Nedergaard[1]

Local increase in blood flow during neural activity forms the basis for functional brain imaging, but its mechanism remains poorly defined. Here we show that cortical astrocytes *in vivo* possess a powerful mechanism for rapid vasodilation. We imaged the activity of astrocytes labeled with the calcium (Ca^{2+})-sensitive indicator rhod-2 in somatosensory cortex of adult mice. Photolysis of caged Ca^{2+} in astrocytic endfeet ensheathing the vessel wall was associated with an 18% increase in arterial cross-section area that corresponded to a 37% increase in blood flow. Vasodilation occurred with a latency of only 1–2 s, and both indomethacin and the cyclooxygenase-1 inhibitor SC-560 blocked the photolysis-induced hyperemia. These observations implicate astrocytes in the control of local microcirculation and suggest that one of their physiological roles is to mediate vasodilation in response to increased neural activity.

Tight spatial and temporal coupling of synaptic activity with local blood flow is a hallmark of brain function[1]. Functional hyperemia occurs within seconds of neuronal activation and is spatially coupled to brain areas with increased energy demands[2,3]. Nevertheless, the mechanisms mediating increases in local perfusion remain poorly understood. Astrocytes are essential for the supply of energy metabolites to neurons and, by means of their processes, provide a physical link to the vasculature[4]. Given this, it is tempting to speculate that astrocytes have a major role in functional hyperemia[5]. Consistent with this, a previous study[5] found that electrical stimulation of cortical slices results in astrocyte activation in an mGluR-dependent pathway triggering release of vasodilatory arachidonic acid metabolites. In contrast, a subsequent study that targeted astrocytes by Ca^{2+} photolysis found that astrocytic Ca^{2+} signaling is associated with cerebrovascular constriction mediated by a cytochrome P-450 metabolite, 20-hydroxy-(5*Z*,8*Z*,11*Z*,14*Z*)-eicosatetraenoic acid (20-HETE)[6]. The seemingly conflicting observations in these studies may be a result of the fact that nonperfused brain slices do not accurately reflect what happens *in vivo*[5].

Here we performed photolysis of caged Ca^{2+} in astrocytic endfeet adjacent to penetrating cortical arteries in live mice so as to define the role of astrocytes in the control of local microcirculation *in vivo*. We found that increases in astrocytic Ca^{2+} were invariably associated with vasodilation. Notably, a cyclooxygenase-1 (COX-1) inhibitor, SC-560, blocked the astrocyte-triggered vasodilation, consistent with high COX-1 immunoreactivity in astrocytic endfeet. In addition, stimulation of neural activity was associated with increased perfusion, which was suppressed by both indomethacin and SC-560. Our observations indicate that astrocytes possess a powerful mechanism for local vasoregulation and are key mediators of functional hyperemia. Moreover, astrocyte-mediated vasodilation was of a similar magnitude in mice anesthetized with ketamine and xylazine, pentobarbital, and urethane and chloralose, indicating that anesthesia may primarily affect neurally mediated mechanisms of functional hyperemia.

RESULTS

Photolysis of caged Ca^{2+} triggers vasodilation

To directly address the role of astrocytes in the control of local microcirculation, we used two-photon imaging of the exposed cortex combined with photolysis of caged Ca^{2+} in anesthetized adult mice. In initial experiments, the exposed cortex was loaded with the acetoxymethyl (AM) ester form of rhod-2 (rhod-2 AM) in mice expressing green fluorescence protein (GFP) under the control of the glial fibrillary acidic protein promoter (GFAP) (GFAP-GFP mice). Rhod-2 and GFP were colocalized, indicating that rhod-2 was preferentially taken up by astrocytes as previously reported for other Ca^{2+} indicators, including fluo-4 AM (**Supplementary Fig. 1** online)[7,8]. In subsequent experiments, rhod-2 AM was loaded together with caged Ca^{2+} and 1-(4,5-dimethoxy-2-nitrophenyl)-EDTA (DMNP-EDTA AM), whereas the vasculature was visualized by the systemic administration of dextran-conjugated fluorescein-5-isothiocyanate (FITC-dextran, molecular weight: 2,000 kDa). Penetrating arteries were followed from pial surface to a depth of 40–50 μm below the cortical surface (**Fig. 1a**). Arteries, as opposed to veins, were identified by the direction of perfusion from the pia. In addition, astrocytic endfeet encasing the arterial wall, and the layer of unlabeled smooth muscle cells, were both thicker than those surrounding veins (**Fig. 1a**). Targeted photolysis of DMNP-EDTA in an astrocytic endfoot contacting an artery triggered spatially restricted Ca^{2+} increases (mean ± s.e.m. = 173.7 ± 29.9%; $n = 28$ experiments, 17 mice) (**Fig. 1b**). The increase in endfoot Ca^{2+} was linked to a marked vasodilation (**Fig. 1b**,**c** and **Supplementary Video 1** online). The mean maximum increase of vessel cross-section area from the baseline was 17.8 ± 2.2% (**Fig. 1d**). Owing to the pulsation and respiration

[1]Center for Aging and Developmental Biology, Department of Neurosurgery, University of Rochester Medical School, 601 Elmwood Avenue, Rochester, New York 14642, USA. [2]Department of Neurosurgery, Jagiellonian University, Cracow, Poland. Correspondence should be addressed to T.T. (Takahiro_Takano@URMC.Rochester.edu).

Received 24 October; accepted 2 December; published online 25 December 2005; doi:10.1038/nn1623

movement artifacts, the cross-section area showed 2.9 ± 1.3% ($n = 10$ with 5 mice) fluctuations during baseline, nonstimulated control conditions (**Fig. 1c,d** and **Supplementary Video 2** online). When the cortex was loaded with only rhod-2 AM (no DMNP-EDTA), similar photostimulation did not trigger a significant increase in astrocytic Ca^{2+} (6.0 ± 2.2%, $n = 12$ with 4 mice) (**Fig. 1c** and **Supplementary Video 3** online). When the photolysis laser power was increased enough to evoke an increase in rhod-2 emission (98.6 ± 26.7%, $n = 4$ with 3 mice) resulting from photodamaging of the cells in mice not loaded with DMNP-EDTA, we noted no significant changes in vessel cross-section area (5.0 ± 2.9%; $P = 0.45$). In a total of 179 recordings, we observed six constriction events (or 3.4% of the total). The constriction averaged –10 ± 2.2% (range: –5.2% to –20% of vessel cross-section area; $n = 6$ with 6 mice) and probably reflected rhythmic fluctuation in vessel diameter[9].

In the next set of experiments, we asked whether the Ca^{2+} increase evoked in the endfeet was restricted to the endfeet or propagated back to the cell soma of the astrocytes. In 16 out of 22 experiments (6 mice), we found that photolysis-induced Ca^{2+} increase remained restricted to the endfeet (**Fig. 2a**). In six experiments, the astrocytic cell soma showed a Ca^{2+} increase, which averaged 47% of the Ca^{2+} increase in the endfeet of the same cells. Notably, vasodilation and the relative increase

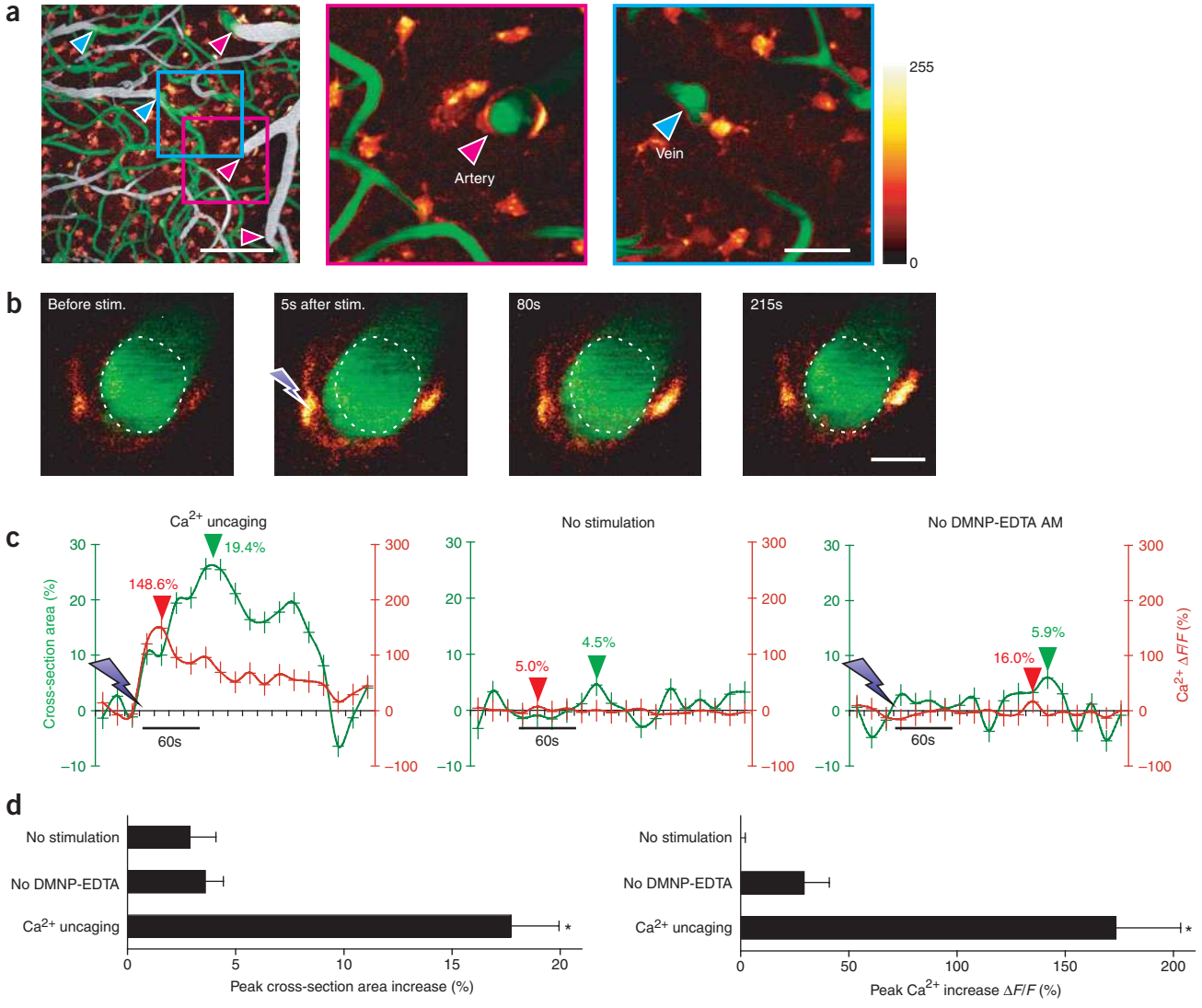

Figure 1 Photolysis of caged Ca^{2+} in astrocytic endfeet triggers vasodilation. (**a**) Left, two-photon microscopy of the cranial window at low magnification. Astrocytes were loaded with the Ca^{2+} indicator dye rhod-2 AM (red) and with DMNP-EDTA AM, whereas the vasculature was stained with FITC-dextran (green). The projection image is composed of serial optical sections collected from 0 μm to 100 μm. Pial vessels at the surface of the brain are shown in white. Red arrows indicate arteries; blue arrows indicate veins. Scale bar, 100 μm. Middle and right, high-magnification view of a penetrating artery and a collecting vein 40 μm below the pial surface as depicted by boxes at left. Scale bar, 30 μm. (**b**) Time-series images of the cross-section of a penetrating artery exposed to photolysis of DMNP-EDTA. Ca^{2+} uncaging triggered a rapid increase of Ca^{2+} in the astrocytic endfoot and arterial vasodilation. Arrow indicates the position of photostimulation. Scale bar, 10 μm. (**c**) Left, time-course tracings show that photostimulation caused a rapid Ca^{2+} increase and arterial vasodilation in the experiment shown in **b**. Omitting photostimulation (middle) or the loading of DMNP-EDTA AM (right) eliminated both the Ca^{2+} increase and the vasodilation. Arrows indicate time of photolysis (purple), peak Ca^{2+} (red) and peak dilation (green). (**d**) Summary histograms of maximum arterial cross-section area (left) and maximum Ca^{2+} increase (right) without photostimulation, with photostimulation but omitting DMNP-EDTA AM loading, and with DMNP-EDTA loading and photolysis. Maximum increase within 1 min after photostimulation was measured relative to baseline before stimulation. Mean ± s.e.m. $^*P < 0.01$ compared to no stimulation; Tukey-Kramer test.

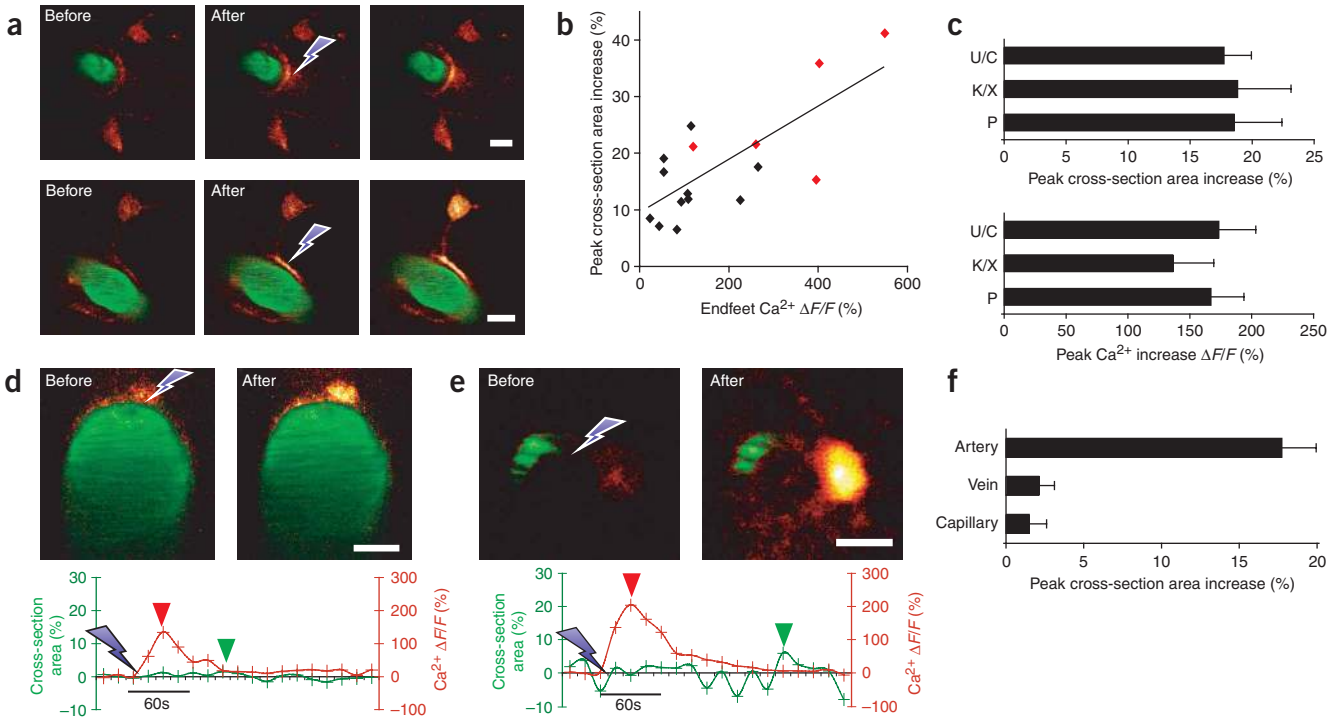

Figure 2 Photolysis-induced vasodilation is a function of the amplitude of endfoot Ca^{2+} and does not occur in veins or capillaries. Astrocytes were loaded with the Ca^{2+} indicator dye rhod-2 AM (red) and with DMNP-EDTA AM, whereas the vasculature was stained with FITC-dextran (green). (**a**) Top, two-photon images of a vascular astrocyte, which showed Ca^{2+} increases restricted to the endfeet after photolysis of caged Ca^{2+}. Arrow indicates the position of photostimulation. Bottom, an astrocyte that showed an increase in both endfoot and somatic Ca^{2+} in response to photolysis of caged Ca^{2+} in the endfoot. Scale bar, 10 μm. (**b**) Vasodilation as a function of the relative increase in Ca^{2+} in astrocytic endfeet ($\Delta F/F$). Black squares indicate experiments in which Ca^{2+} increases remained restricted to the endfeet; red squares indicate experiments with increase in Ca^{2+} in both endfeet and soma. Correlation curve: $y = 0.047x + 9.37$, $R^2 = 0.55$. $n = 16$, 6 mice. (**c**) A summary histogram showing peak increases in vessel cross-section area (top) and Ca^{2+} increase (bottom) with mice anesthetized with urethane and α-chloralose (U/C: 1 g kg^{-1} and 50 mg kg^{-1}, respectively), ketamine and xylazine (K/X: 60 mg kg^{-1} and 10 mg kg^{-1}, respectively), or sodium pentobarbital (P: 90 mg kg^{-1}). Mean ± s.e.m. (**d**) Vein cross-section before and 5 s after Ca^{2+} uncaging in an astrocytic endfoot. The photolysis triggered a transient increase in Ca^{2+}, but not vasodilation. Scale bar, 10 μm. Bottom, time-course tracings of Ca^{2+} in the astrocytic endfoot and the cross-section area of the vein in upper panel. Arrows indicate time of photolysis (purple), peak Ca^{2+} (red) and peak dilation (green). Scale bar, 10 μm. (**e**) Photostimulation of an astrocyte surrounding a capillary resulted in an increase in Ca^{2+}, but the capillary remained unchanged. (**f**) A summary histogram showing peak increases in vessel cross-section area after the uncaging of Ca^{2+} in astrocytic endfeet. Mean ± s.e.m.

in endfeet Ca^{2+} were larger in these 6 experiments compared with the 16 experiments with local increases in endfeet Ca^{2+} (*t*-test: $P = 0.0048$ and $P = 0.0007$, respectively). Thus, the amplitude of Ca^{2+} increases in endfeet may determine the extent of vasodilation. Also, the high increases of Ca^{2+} in endfeet tended to mobilize Ca^{2+} in the soma of vascular astrocytes (**Fig. 2b**).

Anesthetics can influence both vascular tone and responses to stimulation[10–12]. To define whether astrocyte-mediated vasodilation was affected by the choice of anesthetic, we next compared vascular responses in mice anesthetized with urethane and α-chloralose with mice anesthetized with either ketamine and xylazine (60 mg kg^{-1} and 10 mg kg^{-1}, intraperitoneally (i.p.); $n = 19$ with 10 mice) or with sodium pentobarbital (90 mg kg^{-1} i.p.; $n = 25$ with 5 mice). The magnitude of Ca^{2+} increase after photolysis of caged Ca^{2+} in astrocyte endfeet was not significantly different with the different anesthetics (analysis of variance (ANOVA); $P = 0.97$) (**Fig. 2c**). Similarly, astrocyte-induced vasodilation was independent of the choice of anesthetic (ANOVA; $P = 0.67$) (**Fig. 2c**). Thus, the well-documented reliance of activity-dependent increases in blood flow on the type of anesthesia probably reflects direct effects on neural activity[10–12].

Targeted photolysis of Ca^{2+} astrocytic endfeet covering veins or capillaries was not associated with vasodilation: the cross-section area of veins and capillaries increased by 2.12 ± 1.02% ($n = 7$, 2 mice) and 1.49 ± 1.14%, ($n = 9$, 2 mice), respectively, in response to photolysis (**Fig. 2d–f** and **Supplementary Video 4** online). Thus, astrocytic endfeet covering arterial vessel walls possess a unique mechanism for Ca^{2+}-dependent vasodilation.

Vasodilation occurs within seconds after stimulation

One of the defining properties of functional hyperemia is that increases in blood flow occurs only seconds after neuronal stimulation[1,2]. To analyze the temporal dynamics of the photolysis-induced increases in astrocytic Ca^{2+} concentration and vasodilation, we used line scanning with high temporal resolution (2–4 ms per line). Ca^{2+} uncaging resulted in a rapid increase in astrocytic Ca^{2+} and vasodilation (**Fig. 3a–c**). The latency between photolysis and the onset of increments in Ca^{2+} was 0.67 ± 0.11 s, whereas the onset of vasodilation occurred later, at 1.18 ± 0.37 s ($n = 8$ with 3 mice) (**Fig. 3c**). Imaging in line scanning mode showed that vessel expansion resulted from the relaxation of the smooth muscle cells, because the position of the astrocytic endfeet remained stable (**Fig. 3a**, red arrow) whereas the vessel expanded into the space separating the FITC-dextran–filled lumen from the rhod-2–loaded astrocytic endfoot (the smooth muscle cell layer) (**Fig. 3a**, white dashed line).

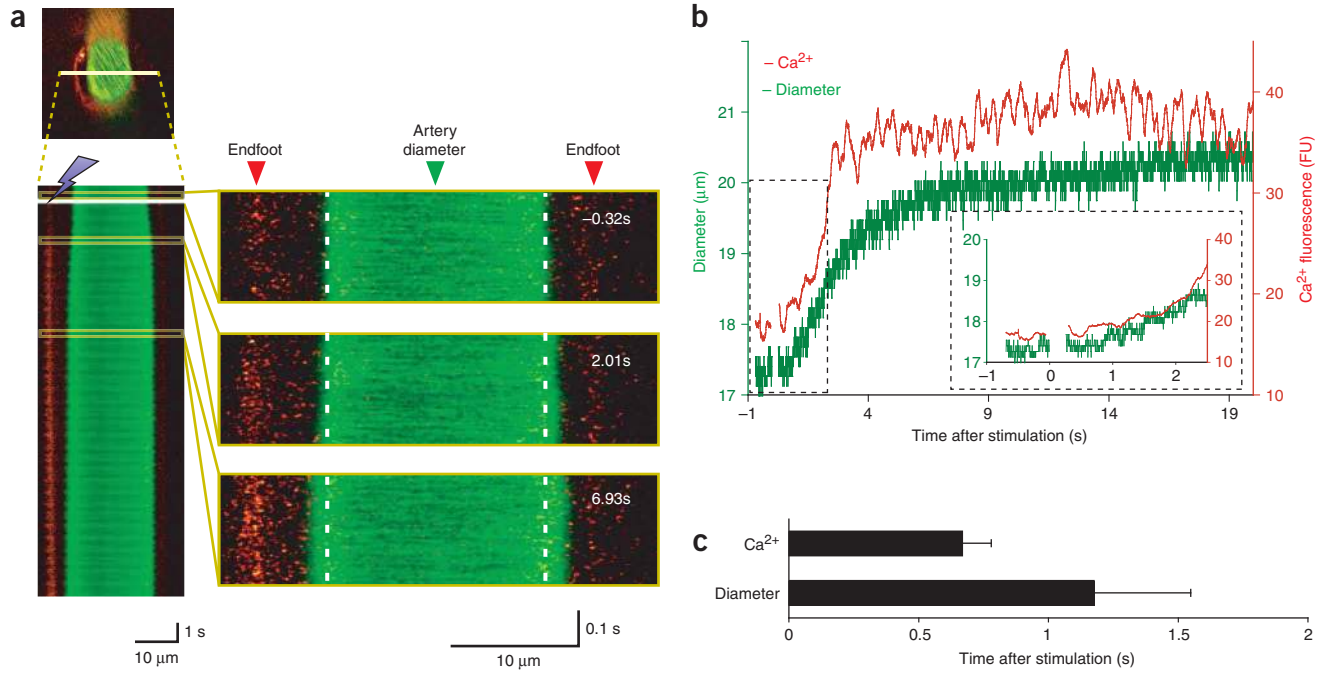

Figure 3 Astrocytes trigger rapid vasodilation (**a**) Top, line scan position across the diameter of an artery. Left, a line scan image of an artery located 40 μm below the pial surface exposed to photolysis of caged Ca^{2+}. A line 34.4 μm in length was scanned at the rate of 3.1 ms per line. Astrocytic Ca^{2+} and the diameter of the inner vessel increased almost simultaneously following photolysis. Right, larger views of line scan section indicated in yellow boxes. (**b**) Time-course tracings of changes in astrocytic Ca^{2+} and arterial diameter in **a**. (**c**) Mean latency in the onset of Ca^{2+} increase vs. mean latency in the onset of vasodilation following photolysis. Mean ± s.e.m.

COX-1 metabolites mediate vasodilation

At least four potential pathways of astrocyte-based vasodilation exist, involving (i) products of the metabolism of the cyclooxygenases COX-1 and COX–2, including prostaglandin E_2 (PGE_2); (ii) epoxygenase pathways, which convert arachidonic acid to vasoactive epoxyeicosatrienoic acids (EETs); (iii) nitric oxide (NO); or (iv) adenosine, a potent vasodilator[1]. To define the intracellular signaling pathway(s), by which astrocytes mediate hyperemia, we first tested the effect of methyl arachidonyl fluorophosphosphonate (MAFP), a phospholipase A_2 (PLA_2) inhibitor[13,14]. As with the other antagonists studied, MAFP was added to the artificial cerebrospinal fluid (aCSF) used for loading rhod-2 AM before imaging. MAFP (500 μM) antagonized photolysis-induced vasodilation by more than 70%, consistent with the high expression of Ca^{2+}-dependent PLA_2 in gray matter astrocytes[15,16] (maximum area change: 5.4 ± 1.9%; $n = 14$ with 4 mice) (**Fig. 4a**).

Cyclooxygenases are rate-limiting enzymes in the conversion of arachidonic acid into prostaglandins and thromboxanes. Astrocytes constitutively express COX-1, whereas COX-2 is not present in the resting state but is expressed in response to inflammatory stimuli including interleukin-1b (IL-1b), exposure to Ca^{2+} ionophores or injury[17]. The fact that MAFP potently inhibited astrocyte-induced vasodilation suggested that arachidonic acid derivatives, produced by astrocytes in response to Ca^{2+} increases, could be the messengers that modulated vascular tone[18]. We obtained support for a role of cyclooxygenase metabolites by observing that a cyclooxygenase inhibitor, indomethacin, attenuated astrocyte-induced vasodilation. In mice exposed to indomethacin (500 μM), photolysis of Ca^{2+} did not induce vasodilation (maximum area change = 4.9 ± 1.4%; $n = 19$ with 3 mice) (**Fig. 4a**,**b** and **Supplementary Video 5** online). Because indomethacin inhibits both COX-1 and COX-2 and has pharmacological effects unrelated to COX inhibition[19], we next evaluated the effect of the selective COX inhibitors. Vasodilation was markedly reduced by a COX-1 inhibitor, SC-560 (500 μM), suggesting a key role of COX-1 in astrocyte-mediated control of vascular tone (maximum area change = 5.1 ± 1.0%; $n = 21$ with 5 mice) (**Fig. 4a** and **Supplementary Video 6** online). In contrast, a specific COX-2 antagonist, NS-398 (600 μM), was ineffective[20] (maximum area change = 17.1 ± 3.9%; $n = 15$ with 6 mice) (**Fig. 4a**). These observations indicate that the Ca^{2+}-induced activation of PLA_2 and the subsequent COX-1 metabolism of arachidonic acid constitute the primary pathway of vasodilation evoked by the photolysis of caged Ca^{2+} in astrocytes. Consistent with the notion that PGE_2 is a potent vasodilator[21], the application of PGE_2 40 μm below the surface (50 mM, pressure-injected by a pipette positioned ~30 μm from the vessel wall) increased the cross-section area of penetrating arteries by 45.3 ± 15.5% (8.64–97.6%, $n = 6$ with 2 mice).

One characteristic of functional hyperemia is that the inhibition of a single pathway does not completely eliminate the response[1,2]. Astrocytes express cytochrome P450 2C11, an epoxygenase that converts arachidonic acid into EETs with both vasodilatory and constrictory effects[22]. We tested the effect of two P450 antagonists, *N*-methylsulfonyl-6-(2-propargyloxyphenyl)-hexanamide (MS-PPOH, a substrate inhibitor[23]) and miconazole (a reversible inhibitor acting on the heme moity[24]). Neither MS-PPOH (200 μM) nor miconazole (500 μM) reduced the vasodilation induced by the photolysis of Ca^{2+} in astrocytes (maximum area change = 13.4 ± 1.5%, $n = 22$ with 5 mice; and 14.2 ± 2.7%, $n = 13$ with 3 mice; respectively) (**Fig. 4a**). Thus, P450 metabolites do not seem to have a significant role in vasodilation compared with COX-1 metabolites. Next, we tested the effect of nitric oxide production. Astrocytes express all three isoforms of nitric oxide synthases[25], and NO mediates, in part, the synaptically induced increases in local blood flow[1,26]. However, N^{ω}-nitro-L-arginine methyl ester (L-NAME, 2 mM), a competitive inhibitor of both

constitutive and inducible nitric oxide synthases, did not reduce astrocyte-induced vasodilation (maximum area change = 15.9 ± 2.8%; $n = 11$ with 3 mice) (**Fig. 4a**). We also asked whether adenosine had a role in photolysis-induced hyperemia. Astrocytes release ATP in response to an increase of cytosolic Ca^{2+}, possibly through the connexin (Cx) hemichannels[27]. ATP is rapidly (time constant = 200 ms) degraded to ADP, AMP and adenosine in the interstitial space[28]. However, astrocyte-mediated vasodilation was insensitive to caffeine (1 mM), a nonspecific inhibitor of the adenosine A1 and A2 receptors, providing no support for a direct role of adenosine or purinergic signaling[29] (maximum area change = 13.2 ± 2.9%; $n = 15$ with 3 mice) (**Fig. 4a**). Notably, an immunohistochemical analysis of the subcellular distribution of COX-1 with antibodies obtained from two independent sources demonstrated that COX-1 was densely expressed in astrocytic endfeet (**Fig. 4c**), as well as in small cells with a morphology typical of microglial cells as previously reported[30]. By contrast, COX-2 expression was not detected along the vessel wall (**Fig. 4c**).

Collectively, our data indicate that COX-1 is the principal mediator of astrocyte-induced vasodilation, consistent with the polarized expression of COX-1 in astrocytic endfeet (**Fig. 4c**). These *in vivo* observations confirm and extend the report that aspirin inhibits astrocyte-mediated vasodilation in cortical slices[18] but not the observation that astrocytes induce vasoconstriction in hippocampal slices[6].

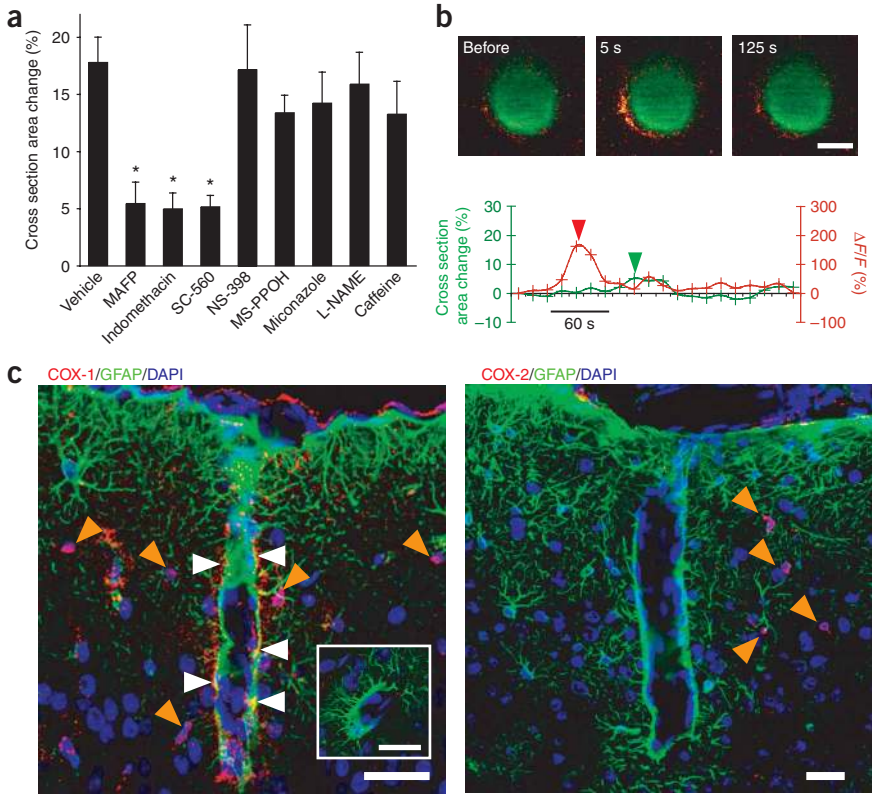

Figure 4 Astrocyte-mediated vasodilation requires COX-1 activity. (**a**) Pharmacology of vasodilation induced by photolysis of caged Ca^{2+} in the astrocytic endfoot. Vasodilation was inhibited by MAFP (0.5 mM), indomethacin (0.5 mM) and a COX-1 inhibitor, SC-560 (0.5 mM). A COX-2 inhibitor, NS-398 (0.6 mM), had no effect. Likewise, an NOS inhibitor, L-NAME (2 mM), the epoxygenase inhibitors MS-PPOH (0.2 mM) and miconazole (0.5 mM), and an adenosine receptor antagonist, caffeine (1 mM), did not reduce arterial dilation. Mean ± s.e.m. $^*P < 0.01$; Tukey-Kramer test. (**b**) Top, time-course images of an artery (FITC-dextran, green) and surrounding astrocytic endfeet (rhod-2, red). The exposed cortex was loaded with rhod-2 AM, DMNP-EDTA AM and indomethacin (0.5 mM). Photolysis-induced increases in astrocytic Ca^{2+} did not trigger vasodilation in the presence of indomethacin. Scale bar, 10 μm. Bottom, time-course tracings of changes in astrocytic Ca^{2+} and arterial cross-section area in the upper panel. (**c**) Immunohistochemistry images of a cortical section stained with DAPI (blue), GFAP (green) and COX-1 (left panel, red) or COX-2 (right panel, red). Astrocytic endfeet surrounding a penetrating artery (white arrows) showed high COX-1 expressions, whereas COX-2 was absent around penetrating arteries. High COX-1 and COX-2 expression were evident in small GFAP-negative cells with morphology similar to microglial cells (orange arrows). Inset: incubation of the COX-1 antibody with the presence of the blocking peptide eliminated staining of both the vessels and the presumed microglial cells. Scale bars, 30 μm.

Neural activity increases astrocytic Ca^{2+} and blood flow

To establish whether arachidonic acid metabolites contribute to synapse-mediated hyperemia, we next triggered local increases in cortical neural activity with a bipolar electrode placed 400–600 μm below the pial surface. Electrical stimulation evoked an increase in neural activity and a widespread increase in astrocytic Ca^{2+} ($n = 15$ with 5 mice), and was also associated with vasodilation (**Fig. 5a**). This electrical stimulation–evoked vasodilation was reduced by indomethacin (500 μM) whereas the Ca^{2+} signaling was unaffected ($n = 15$ with 5 mice) (**Fig. 5b,c**). As an alternative approach to detecting changes in local blood flow, we next used laser Doppler flowmetry. The increase in blood flow evoked by electrical stimulation averaged 45.4 ± 1.9% ($n = 16$ with 16 mice) of baseline values and was sustained during the 1-min stimulation period (**Fig. 5d**). Blood flow returned to baseline within 30–40 s after the cessation of stimulation (**Fig. 5d**). Indomethacin reduced, but did not eliminate, the increase in local perfusion evoked by electrical stimulation. On average, electrical stimulation resulted in a 27.7 ± 5.1% ($n = 4$ with 4 mice) increase in blood flow after treatment with indomethacin (500 μM) and a 40% reduction in the increase in local perfusion compared with that in vehicle-treated controls (**Fig. 5d,e**). Indomethacin reduces blood flow–synaptic activity coupling[31–33]. Furthermore, the COX-1 inhibitor SC-560 (500 μM) reduced hyperemia by more than 50% (21.9 ± 2.1%, $n = 4$ with 4 mice) compared to baseline (**Fig. 5e**). To establish whether synaptic glutamatergic activity was required for the hyperemia evoked by electrical stimulation, we administered the blood-brain barrier–permeable AMPA receptor antagonist 6-cyano-7-nitroquinoxaline-2,3-dione (CNQX). CNQX (30 mg kg^{-1}, intravenously (i.v.)) reduced field potential to 27.7 ± 3.8% and hyperemia by almost 70% to 14.6 ± 2.6% ($n = 4$ with 4 mice), confirming previous reports that glutamatergic synaptic transmission is required for activity-dependent increases in blood flow[1] (**Fig. 5e,f**). Therefore neuron to astrocyte signaling is, at least in part, mediated by the synaptic release of glutamate, which triggers increase in astrocytic Ca^{2+} by an mGluR5 receptor–dependent pathway[18,34]. In accordance with these observations, we found that the mGluR5 antagonist 6-methyl-2-(phenylethynyl)-pyridine (MPEP, 10 mg kg^{-1}, i.v.) reduced vascular responses to

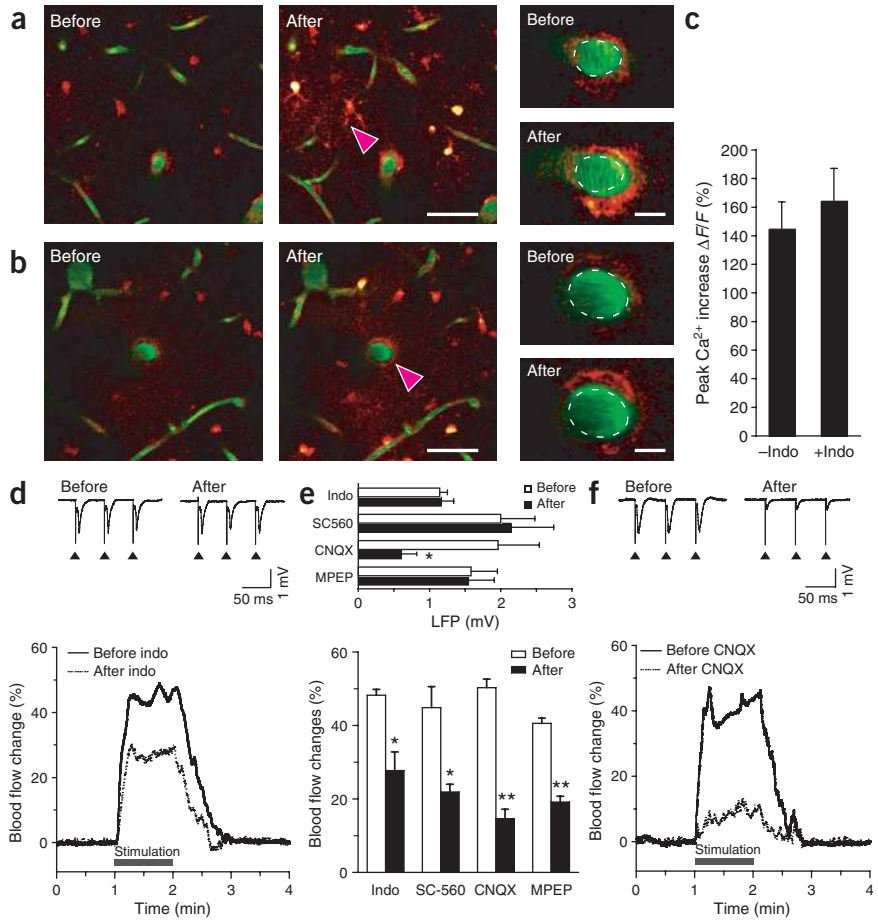

Figure 5 Increased neuronal activity triggers astrocytic Ca^{2+} signaling and indomethacin-sensitive vasodilation. (**a**) Electrical stimulation is associated with a widespread increase in astrocytic Ca^{2+} concentration and vasodilation. Left, low-magnification images 60 μm below the pial surface showing the general increase in astrocytic Ca^{2+} that occurred in response to electrical stimulation. Scale bar, 50 μm. Right, the penetrating artery indicated by the red arrow in the left panel showed an increase in vessel cross-section area in response to stimulation. Scale bar, 10 μm. (**b**) Left, exposure to indomethacin (0.5 mM) did not reduce the Ca^{2+} increase evoked by electrical stimulation. Right, the penetrating artery indicated by the red arrow in the left panel showed a smaller increase in response to stimulation. (**c**) A summary histogram showing that maximum Ca^{2+} increase was not altered by indomethacin. Mean ± s.e.m. $P = 0.51$, *t*-test. (**d**) Top, stimulation-evoked local extracellular synaptic field potentials (LFP) were not altered by the presence of indomethacin. Bottom, relative increase in blood flow detected by laser Doppler after electrical stimulation. Indomethacin (0.5 mM) decreased, but did not abolish the increase in, blood flow. (**e**) Summary histograms of LFP (above) and the relative changes in blood flow detected by laser Doppler (below) in the same mice before and after treatment with indomethacin (500 μM), SC-560 (500 μM), CNQX (30 mg kg^{-1}, i.v.) or MPEP (10 mg kg^{-1}, i.v.). Mean ± s.e.m. $^*P < 0.05$: $^{**}P < 0.001$, paired *t*-test. (**f**) CNQX (30 mg kg^{-1}, i.v.) reduced both extracellular synaptic field potentials and blood flow increase in response to electrical stimulation.

electrical stimulation by almost 50%, to 20.8 ± 3.7% ($n = 4$ with 4 mice), without altering synaptic responses (98.7 ± 4.0%) (**Fig. 5e**).

Collectively, our observations indicate that increased synaptic activity was associated with widespread increase of astrocytic Ca^{2+} and an increase in local perfusion. Activity-dependent hyperemia was reduced when synaptic transmission was inhibited by the AMPA receptor antagonist CNQX. Moreover, the involvement of astrocytes was demonstrated by the fact that the mGluR5 antagonist MPEP reduced blood flow change in the absence of an effect on neural activity. In addition, local hyperemia was reduced by 40–50% by indomethacin and SC-560, supporting the notion that astrocytic Ca^{2+} signaling and release of COX-1 metabolic products partly mediate the activity-dependent increases in local blood flow.

DISCUSSION

The major advance of this study is that we were able to isolate the role of astrocytes in the control of local microcirculation by using targeted stimulation. We showed that astrocytes in adult mice possess a powerful mechanism for local vasodilation. Selective increase of Ca^{2+} in astrocytic endfeet was consistently associated with vasodilation. Vessel cross-sectional area was increased by ~18%, which corresponded to a 37% increase in flow rate (see Methods). Vasodilation occurred rapidly, with a mean delay of 1.2 s after photolysis and only 0.6 s after the rise in cytosolic Ca^{2+}. The diameters of the vessels typically returned to their prestimulation values after a couple of minutes. Several lines of evidence are consistent with the notion that astrocyte-mediated vasodilation depends primarily on COX-1 metabolites. PGE_2 triggered hyperemia, and both indomethacin and the COX-1 inhibitor SC-560 potently blocked dilation. Immunohistochemical analysis revealed a high expression of COX-1 in astrocytic endfeet in contact with penetrating cortical arteries, in addition to the previously reported[30] high COX-1 expression in microglial cells. By contrast, no COX-2 immunolabeling was evident around the vasculature, and the COX-2 inhibitor did not reduce vasodilation evoked by the photolysis of caged Ca^{2+} in astrocyte endfeet. Similarly, inhibitors of another metabolic cascade of arachidonic acid, the P450 pathways, had no effect on photolysis-induced vasodilation. Furthermore, our observations did not support a role of nitric oxide production or adenosine in astrocyte-mediated vasodilation. Thus, the Ca^{2+}-dependent activation of PLA_2 leads to vasodilation through the release of COX-1 metabolites from astrocytic endfeet. Additional experiments showed that stimulation of neural activity caused a prompt increase in astrocytic Ca^{2+} associated with vasodilation. Indomethacin and the COX-1 inhibitor SC-560 only partly suppressed functional hyperemia, in accordance with the idea that additional pathways probably contribute to activity-dependent increases in blood flow[2].

Our study supports previous conclusions[6] that astrocytic Ca^{2+} increases are associated with vasodilation in a pathway mediated by arachidonic acid metabolic products[6]. However, our study differs from previous studies on several critical issues. First and most important, we studied live, exposed cortex of adult mice, whereas previous studies have used brain slices prepared from mouse pups (postnatal day 9–18)[6,9,18]. Second, photolysis of astrocytic endfeet triggered almost instantaneous vasodilation (1–2 s), whereas a delay averaging 33 s was noted in slice preparations[18]. No simple explanation can be given for

the discrepancy, but it is likely that the absence of blood flow and arterial pressure in slice preparations as well as reduced synaptic activity and metabolic demands could alter normal physiological responses[35].

The neurovascular unit represents the interface between the CNS and the vascular system[36]. In addition to its barrier function, it has important roles in the regulated entry of substrates and exit of waste products and in the regulation of local microcirculation. The brain is a metabolically active organ, and synaptic activity is intimately linked to increases in local blood flow, which occur within the remarkably short time frame of seconds[1]. The tight coupling of blood flow to metabolism is maintained during sleep and deep inhalation anesthesia, and its disappearance is linked to severe pathology, including subarachnoid bleeding, stroke, hypotension and traumatic brain injury[37]. Functional magnetic resonance imaging (fMRI) is widely used in brain activation studies and is based on the detection of the blood oxygen level–dependent signal (BOLD). Activity-dependent changes in the BOLD signal result from increased perfusion and blood volume, suggesting that the activation of astrocytes contributes to the changes observed in functional imaging studies[2]. Notably, an early sign of Alzheimer's disease is the significantly reduced changes in the BOLD signal during the execution of mental tasks and in response to external stimulation[38–40]. Also, transgenic mice overexpressing amyloid precursor protein (APP) show a profound attenuation of functional hyperemia in response to whisker stimulation[41]. Chronic inability to increase blood flow in response to increased energy demands may, in the long term, contribute to neuronal dysfunction and death[1,42]. Our study suggests that astrocytes may be critically involved in the coupling of metabolism and blood flow and, as such, in the pathologies involving abnormal control of cerebral microcirculation.

METHODS

Animal preparation. We anesthetized 8- to 10-week-old male FVB/NJ mice (Jackson Laboratory) with a mixture of ketamine (60 mg kg^{-1}, i.p.) and xylazine (10 mg kg^{-1}, i.p.), and catheterized a femoral artery. Then we made a craniotomy (3 mm in diameter) over the primary somatosensory cortex, centered 1–2 mm posterior to the bregma and 2–3 mm from the midline, and removed the dura. We glued a custom-made metal plate to the skull with dental acrylic cement. We dissolved rhod-2 AM (Invitrogen, 2 mM, 1 h) and DMNP-EDTA AM (Invitrogen, 200 μM, 1 h) in aCSF containing 126 mM NaCl, 2.5 mM KCl, 1.25 mM NaH_2PO_4, 2 mM $MgCl_2$, 2 mM $CaCl_2$, 10 mM glucose and 26 mM $NaHCO_3$ at pH 7.4, gassed with 95% O_2 and 5% CO_2 (refs. 7,8). The incubation was followed by a 10-min wash with aCSF. We poured aCSF containing 1% agarose onto the craniotomy and mounted a coverslip (5 mm in diameter). The mice were intubated and artificially ventilated with a mixture of 70% nitrogen and 30% oxygen using a small-animal ventilator (SAR-830, CWE) set to 100 breath min^{-1} with tidal volume of 0.3–0.4 ml. After the surgery, the mouse was allowed to recover, then reanesthetized with urethane and α-chloralose (1 g kg^{-1} and 50 mg kg^{-1} i.p., respectively). Urethane and α-chloralose were used in all experiments except for those with various other anesthetic treatments (**Fig. 2c**). In these experiments, the mice were reanesthetized with either ketamine and xylazine (60 mg kg^{-1} and 10 mg kg^{-1} i.p., respectively) or sodium pentobarbital (90 mg kg^{-1}, i.p.). FITC-dextran (2,000 kDa, 5%) was systemically administered. We analyzed blood gases, p_{CO_2}, p_{O_2} and pH in microsamples (Rapidlab 248, Bayer, 40-μl samples). Body temperature was monitored by a rectal probe and maintained at 37 °C by a heating blanket (T/PUMP, Gaymer). Experiments were completed only if the physiological variables remained within normal limits. The normal limits for p_{CO_2} and p_{O_2} were set at 30–35 mm Hg and100–150 mm Hg, respectively, and arterial blood pH was set at 7.3–7.35. The antagonists were dissolved in aCSF and applied together with rhod-2 AM for 1 h; this was followed by a 15-min wash with aCSF containing the antagonist. We calculated that the effective drug concentration was ten times lower than if the drug had been used in slice preparations, in accordance with a recent publication[43]. CNQX and MPEP were administered i.v. PGE_2 was delivered by pressure injection (10 p.s.i., 50-ms puffs delivered by Picospritzer III, Parker), by a micropipette (2-μm tip diameter; 50-mM PGE_2) placed within 30 μm from the vessel wall. MAFP, SC-560 and NS-398 were purchased from Cayman Chemical. MS-PPOH was a gift from J.R. Falck (University of Texas Southwestern Medical Center, Texas). All experiments were approved by the Institution Animal Care and Use Committee of University of Rochester.

***In vivo* two-photon imaging and photolysis.** We used a custom-built microscope attached to a Tsunami/Millenium laser (SpectraPhysics) and a scanning box (FV300, Olympus) using Fluoview software for two-photon imaging. We used a 40× water-immersion objective lens with NA 0.80 (LUMPlanFI/IR, Olympus). FITC-dextran and rhod-2 AM were excited at 825 nm, and we detected emitted light with 525/50 and 607/45 filters. Laser power was lowered to 5–10 mW (at the specimen) to avoid photostimulation of astrocytes (**Supplementary Fig. 2** online). *Gfap*^{GFP} transgenic mice (Jackson Laboratory) loaded with rhod-2 AM were visualized at 880-nm excitation. We visualized pial arteries and veins under a bright field and identified penetrating arteries or collecting veins (10–35 μm diameter) by following the direction of flow from the pial surface. Capillaries were identified by their diameter (<5 μm). Photolysis was carried out by giving three pulses of 355-nm laser (DPSS laser) controlled by a shutter (Uniblitz, Vincent Associate, 10-ms duration with an interval of 50 ms) targeted to an endfoot of a single astrocyte surrounding vessels. For line scans, a line was placed along the vessel diameter, and a continuous line scan of typically 2–4 ms per line (depending on the length of the line chosen for line scanning) was captured during photolysis events, except for a brief interruption of 100–150 ms during the photolysis light flash to protect photomultipliers from exposure to high-intensity light. In all the experiments, we imaged vessels located 40–60 μm below the pial surface. Vessel cross-section area and rhod-2 emission were quantified using ImageJ software (NIH). We measured Ca^{2+} increase as the relative increase of fluorescence from the baseline intensity ($\Delta F/F$). The change in blood flow rate in a single vessel was calculated using the Poiseuille equation: $Q = \frac{\pi r^4}{8\eta L}\Delta P$, where Q is the flow rate through the vessel, P is the pressure drop across the vessel, r is the inner radius, L is the length and η is the blood viscosity ($\eta = 3.5$ centipoise; ref. 44). Radius was defined as the square root of cross-sectional area divided by π.

Electrical stimulation and laser Doppler. We anesthetized mice, ventilated them and made a craniotomy over the primary somatosensory cortex as described above. We placed a coated bipolar tungsten electrode (TST33A05KT, WPI) 400–600 μm below the cortical surface and applied pulses of 200-μs constant current with an intensity of 50 μA (ISO-Flex, AMPI) at a frequency of 20 Hz. We recorded the Ca^{2+} activity in astrocytes 40–60 μm from the surface directly above the stimulation electrode. To quantify the Ca^{2+} increase, we randomly chose ten areas devoid of vessels in each field of the image sequences. For field potential recording, we filled the pipette with 2-M NaCl (2–3 MΩ) and placed it at a depth of 100 μm in the cortex. Recording signals were obtained with a multiclamp 700A amplifier (Axon), filtered at a cutoff frequency of 1 kHz and sampled, at intervals of 200 μs, by a pCLAMPEX 9.2 program and DigiData 1332A interface (Axon). Relative changes in local perfusion were detected by laser Doppler flowmetry (PF5010 Laser Doppler Perfusion Module with microtips, PR 418-1, Perimed). The tip of the fiber probe was placed directly on the cortical surface of an area devoid of large vessels. Signals were analog-to-digital converted with the DigiData 1332A interface (with an interval of 200 μs) and recorded with a pCLAMPEX 9.2 program. For each mouse, we recorded both before and after the administration of antagonists.

Immunohistochemistry. Coronal 15-μm-thick cryostat sections of brain slices of adult male mice were prepared as described in a previous study[45]. Sections were stained with either a polyclonal antibody to COX-1 or COX-2 (SC-1747, 1:100, Santa Cruz Biotechnology) and a monoclonal antibody to GFAP (G3893, 1:400, Sigma); or a monoclonal antibody to COX-1 (160,110, 1:100, Cayman Chemical) and a polyclonal antibody to GFAP (ab4674, 1:50 ABCam). In some sections, the blocking peptide for the COX-1 antibody was preincubated with the polyclonal antibody (5:1, in 4 °C for 24 h) before incubating with the tissue. After the immunolabeling, the section was counter-stained with 4,6-diamidino-2-phenylindole (DAPI, D-21490, 1:10,000, Invitrogen), and the images were collected with a confocal microscope (FV500, Olympus).

Note: Supplementary information is available on the Nature Neuroscience website.

ACKNOWLEDGMENTS

We thank M. Lauritzen, B. Zlokovic and L. Bekar for comments on the manuscript; M. Schwartzman and K. O'Banion for discussions; and J.R. Falck for supplying us with MS-PPOH. This work was sponsored by the US National Institutes of Health and National Institute of Neurological Disorders and Stroke.

COMPETING INTERESTS STATEMENT

The authors declare that they have no competing financial interests.

Published online at http://www.nature.com/natureneuroscience/
Reprints and permissions information is available online at http://npg.nature.com/reprintsandpermissions/

1. Iadecola, C. Neurovascular regulation in the normal brain and in Alzheimer's disease. *Nat. Rev. Neurosci.* **5**, 347–360 (2004).
2. Lauritzen, M. Reading vascular changes in brain imaging: is dendritic calcium the key? *Nat. Rev. Neurosci.* **6**, 77–85 (2005).
3. Chaigneau, E., Oheim, M., Audinat, E. & Charpak, S. Two-photon imaging of capillary blood flow in olfactory bulb glomeruli. *Proc. Natl. Acad. Sci. USA* **100**, 13081–13086 (2003).
4. Simard, M., Arcuino, G., Takano, T., Liu, Q.S. & Nedergaard, M. Signaling at the gliovascular interface. *J. Neurosci.* **23**, 9254–9262 (2003).
5. Hirase, H. A multi-photon window onto neuronal-glial-vascular communication. *Trends Neurosci.* **28**, 217–219 (2005).
6. Mulligan, S.J. & MacVicar, B.A. Calcium transients in astrocyte endfeet cause cerebrovascular constrictions. *Nature* **431**, 195–199 (2004).
7. Hirase, H., Qian, L., Bartho, P. & Buzsaki, G. Calcium dynamics of cortical astrocytic networks *in vivo*. *PLoS Biol.* **2**, E96 (2004).
8. Tian, G.F. *et al.* An astrocytic basis of epilepsy. *Nat. Med.* **11**, 973–981 (2005).
9. Filosa, J.A., Bonev, A.D. & Nelson, M.T. Calcium dynamics in cortical astrocytes and arterioles during neurovascular coupling. *Circ. Res.* **95**, 73–81 (2004).
10. Ueki, M., Mies, G. & Hossmann, K.A. Effect of alpha-chloralose, halothane, pentobarbital and nitrous oxide anesthesia on metabolic coupling in somatosensory cortex of rat. *Acta Anaesthesiol. Scand.* **36**, 318–322 (1992).
11. Lindauer, U., Villringer, A. & Dirnagl, U. Characterization of CBF response to somatosensory stimulation: model and influence of anesthetics. *Am. J. Physiol.* **264**, H1223–H1228 (1993).
12. Gordon, E.L., Meno, J.R., Ngai, A.C., Lam, A.M. & Winn, H.R. Anesthetic-dependent pial arteriolar response to ethanol. *J. Neurosurg.* **83**, 875–877 (1995).
13. Farooqui, A.A., Yang, H.C., Rosenberger, T.A. & Horrocks, L.A. Phospholipase A2 and its role in brain tissue. *J. Neurochem.* **69**, 889–901 (1997).
14. Xu, J. *et al.* Prostaglandin E2 production in astrocytes: regulation by cytokines, extracellular ATP, and oxidative agents. *Prostaglandins Leukot. Essent. Fatty Acids* **69**, 437–448 (2003).
15. Stephenson, D.T. *et al.* Calcium-sensitive cytosolic phospholipase A2 (cPLA2) is expressed in human brain astrocytes. *Brain Res.* **637**, 97–105 (1994).
16. Xu, J., Yu, S., Sun, A.Y. & Sun, G.Y. Oxidant-mediated AA release from astrocytes involves cPLA(2) and iPLA(2). *Free Radic. Biol. Med.* **34**, 1531–1543 (2003).
17. Hurley, S.D., Olschowka, J.A. & O'Banion, M.K. Cyclooxygenase inhibition as a strategy to ameliorate brain injury. *J. Neurotrauma* **19**, 1–15 (2002).
18. Zonta, M. *et al.* Neuron-to-astrocyte signaling is central to the dynamic control of brain microcirculation. *Nat. Neurosci.* **6**, 43–50 (2003).
19. Niwa, K., Haensel, C., Ross, M.E. & Iadecola, C. Cyclooxygenase-1 participates in selected vasodilator responses of the cerebral circulation. *Circ. Res.* **88**, 600–608 (2001).
20. Niwa, K., Araki, E., Morham, S.G., Ross, M.E. & Iadecola, C. Cyclooxygenase-2 contributes to functional hyperemia in whisker-barrel cortex. *J. Neurosci.* **20**, 763–770 (2000).
21. Ellis, E.F., Wei, E.P. & Kontos, H.A. Vasodilation of cat cerebral arterioles by prostaglandins D2, E2, G2, and I2. *Am. J. Physiol.* **237**, H381–H385 (1979).
22. Harder, D.R., Campbell, W.B. & Roman, R.J. Role of cytochrome P-450 enzymes and metabolites of arachidonic acid in the control of vascular tone. *J. Vasc. Res.* **32**, 79–92 (1995).
23. Wang, M.H. *et al.* Cytochrome P450-derived arachidonic acid metabolism in the rat kidney: characterization of selective inhibitors. *J. Pharmacol. Exp. Ther.* **284**, 966–973 (1998).
24. Peng, X. *et al.* Suppression of cortical functional hyperemia to vibrissal stimulation in the rat by epoxygenase inhibitors. *Am. J. Physiol. Heart Circ. Physiol.* **283**, H2029–H2037 (2002).
25. Gibson, C.L., Coughlan, T.C. & Murphy, S.P. Glial nitric oxide and ischemia. *Glia* **50**, 417–426 (2005).
26. Yang, G., Chen, G., Ebner, T.J. & Iadecola, C. Nitric oxide is the predominant mediator of cerebellar hyperemia during somatosensory activation in rats. *Am. J. Physiol.* **277**, R1760–R1770 (1999).
27. Cotrina, M.L. *et al.* Connexins regulate calcium signaling by controlling ATP release. *Proc. Natl. Acad. Sci. USA* **95**, 15735–15740 (1998).
28. Dunwiddie, T.V., Diao, L. & Proctor, W.R. Adenine nucleotides undergo rapid, quantitative conversion to adenosine in the extracellular space in rat hippocampus. *J. Neurosci.* **17**, 7673–7682 (1997).
29. Dunwiddie, T.V. & Masino, S.A. The role and regulation of adenosine in the central nervous system. *Annu. Rev. Neurosci.* **24**, 31–55 (2001).
30. Yermakova, A.V., Rollins, J., Callahan, L.M., Rogers, J. & O'Banion, M.K. Cyclooxygenase-1 in human Alzheimer and control brain: quantitative analysis of expression by microglia and CA3 hippocampal neurons. *J. Neuropathol. Exp. Neurol.* **58**, 1135–1146 (1999).
31. Sakabe, T. & Siesjo, B.K. The effect of indomethacin on the blood flow-metabolism couple in the brain under normal, hypercapnic and hypoxic conditions. *Acta Physiol. Scand.* **107**, 283–284 (1979).
32. Bruhn, H., Fransson, P. & Frahm, J. Modulation of cerebral blood oxygenation by indomethacin: MRI at rest and functional brain activation. *J. Magn. Reson. Imaging* **13**, 325–334 (2001).
33. Bakalova, R.A., Matsuura, T. & Kanno, I. Cyclooxygenase-pathway participates in the regulation of regional cerebral blood flow in response to neuronal activation under normo- and hypercapnia. *Prostaglandins Leukot. Essent. Fatty Acids* **67**, 379–388 (2002).
34. Parri, H.R., Gould, T.M. & Crunelli, V. Spontaneous astrocytic Ca^{2+} oscillations *in situ* drive NMDAR-mediated neuronal excitation. *Nat. Neurosci.* **4**, 803–812 (2001).
35. Anderson, C.M. & Nedergaard, M. Astrocyte-mediated control of cerebral microcirculation. *Trends Neurosci.* **26**, 340–344; author reply 344–345 (2003).
36. del Zoppo, G.J. & Hallenbeck, J.M. Advances in the vascular pathophysiology of ischemic stroke. *Thromb. Res.* **98**, 73–81 (2000).
37. Vavilala, M.S., Lee, L.A. & Lam, A.M. Cerebral blood flow and vascular physiology. *Anesthesiol. Clin. N. Am.* **20**, 247–264 (2002).
38. Smith, C.D. *et al.* Altered brain activation in cognitively intact individuals at high risk for Alzheimer's disease. *Neurology* **53**, 1391–1396 (1999).
39. Grossman, M. *et al.* Neural basis for verb processing in Alzheimer's disease: an fMRI study. *Neuropsychology* **17**, 658–674 (2003).
40. Rombouts, S.A., Barkhof, F., Van Meel, C.S. & Scheltens, P. Alterations in brain activation during cholinergic enhancement with rivastigmine in Alzheimer's disease. *J. Neurol. Neurosurg. Psychiatry* **73**, 665–671 (2002).
41. Niwa, K. *et al.* Cerebrovascular autoregulation is profoundly impaired in mice overexpressing amyloid precursor protein. *Am. J. Physiol. Heart Circ. Physiol.* **283**, H315–H323 (2002).
42. Zlokovic, B.V. Neurovascular mechanisms of Alzheimer's neurodegeneration. *Trends Neurosci.* **28**, 202–208 (2005).
43. Davalos, D. *et al.* ATP mediates rapid microglial response to local brain injury *in vivo*. *Nat. Neurosci.* (2005).
44. Hademenos, G.J., Massoud, T.F. & Vinuela, F. A biomathematical model of intracranial arteriovenous malformations based on electrical network analysis: theory and hemodynamics. *Neurosurgery* **38**, 1005–1015 (1996).
45. Wang, X. *et al.* P2X7 receptor inhibition improves recovery after spinal cord injury. *Nat. Med.* **10**, 821–827 (2004).